Supporting Information

Shell-Switchable SERS Blocking Strategy for Quantitative Copper Ion Detection using Single Particle SERS Probes

Longteng Liang[a,b], Yingqing Zhu[a], Anran Wang[a], Lixia Li[a], Ning Feng[a], Yufang Liu[a,b*]*

[a]Henan Key Laboratory of Infrared Materials Spectrum Measures and Applications, School of Optoelectronic Engineering, Henan Normal University, Xinxiang 453007, China

[b]Institute of Physics, Henan Academy of Sciences, Zhengzhou 450046, China

[*]Address correspondence to: fengning@htu.edu.cn; yf-liu@htu.edu.cn

1. Experimental Procedures

1.1 Materials

Cetyltrimethylammonium bromide (CTAB), cetyltrimethylammonium chloride (CTAC), gold chloride ($HAuCl_4$), sodium borohydride ($NaBH_4$), ascorbic acid (AA), 1,4-Benzenedithiol (1,4-BDT), copper chloride ($CuCl_2$), potassium iodide (KI), ethylenediaminetetraacetic acid (EDTA), and 3-mercaptopropyltriethoxysilane (MPTES) were purchased from Sigma-Aldrich. Milli-Q water (18.2 MΩ cm) was used in all experiments. All materials were used as received without any further purification.

1.2 Instrumentation

Transmission electron microscope (TEM) images were acquired from a JEM-F200 instrument (Japan). Extinction spectra were obtained with an ideaoptics NAVO2S spectrophotometer.

The dark-field microscopy (DFM) images, localized surface plasmon resonance

(LSPR) and SERS scattering spectrum measurements were recorded by an inverted microscope (eclipse Ti2-U, Nikon) equipped with a monochromator (Acton SP2358), a -75 °C cooled CCD detector (PIXIS 400BR: excelon, Princeton Instruments) and a 785 nm continuous-wave laser light (Spectra-Physics Excelsior, 100 mW). The microscope was equipped with a 60X objective lens (NA=0.70), a dark-field condenser (0.8 < numerical aperture (NA) < 0.95), and a true-color digital camera (Nikon DS-fi2). The spectra were integrated through a 1 μm slit width.

1.3 Synthesis of Au cores

Au cores were synthesized using a seed-mediated process.[1] Typically, seed solution was firstly prepared by vigorous mixing of 5 mL of aqueous CTAB solution (0.2 M), 4.5 mL water and 515 μL of $HAuCl_4$ (4.86 mM) with 450 μL of $NaBH_4$ solution (0.02 M). The seed solution was allowed to stay at 30°C for 1 hour in a hot bath and further diluted by 10 times. Then 10 mL of CTAB solution (0.1 M) was mixed with 515 μL of $HAuCl_4$ (4.86 mM) and 75 μL of ascorbic acid (0.04 M). 100 μL of diluted seed solution was added into the solution under sonication and kept undisturbed under darkness for two days to obtain highly uniform spherical nanoparticles. The size of the Au cores obtained at this stage was about 20 nm.

1.4 Synthesis of BRIGHTs

The obtained CTAB-capped Au cores (10 mL) were mixed with 400 μL of 1,4-BDT solution (2 mM) under vigorous sonication for 20 minutes. These modified cores were then washed for three times to remove excess reagent, and further dispersed in 5 mL aqueous CTAC solution (0.1 M). The Au core-shell nanoparticles was prepared by

adding 150 μL of 1,4-BDT modified core solution into the mixture of 2 mL CTAC solution (0.1 M), 60 μL of ascorbic acid (0.04 M), and 120 μL of $HAuCl_4$ (4.86 mM) under vigorous sonication. Finally, the gold particles were washed for three times and stored in aqueous CTAC solution (0.1 M).

1.5 Characterization of SERS spectrum

The SERS spectrum of individual nanoparticle was performed by using the DFM-correlated Raman spectroscopy setup (Fig. S1). Briefly, the position of the individual particle was located by using the DFM image, following the light pathway was switched with a laser source instead of the white light, and then the corresponding SERS spectra were captured by using Raman spectroscopy. In this study, the SERS spectrum of individual core-shell nanostructure was collected at an excitation wavelength of 785 nm, 0.5 mW of laser power and captured for 10 seconds. Throughout this work, for each experimental condition or concentration point, Raman spectra were acquired from at least 30 individual BRIGHTs (10 particles from each of three independently prepared samples) to ensure statistical reliability. The total measurement time per condition, including particle localization and spectral acquisition, was approximately 60 minutes. Fig. S4B depicts a typical SERS spectrum detected from individual core-shell nanostructure. The characteristic Raman peak of 1,4-BDT at 1055 and 1555 cm^{-1}, which are assigned to the phenyl ring breathing mode (CH in-plane bending and CS stretching) and the phenyl ring stretching motion (8a vibrational mode), can be seen clearly.[2-4]

1.6 SERS enhancement factor estimation

Sparsely distributed individual BRIGHTs were identified using dark-field optical

microscopy and SERS spectra were collected from individual nanostructures. Raman spectrometer mounted on a Nikon microscope with 60× objective (NA = 0.7) in the range of 300-1800 cm^{-1} with one accumulation and 10 s exposure time. A 785 nm wavelength diode laser (0.5 mW) was used to excite the sample. The following expression was used to calculate the enhancement factor (EF) of SERS substrate at 1555 cm^{-1} band:

$$EF = \frac{I_{SERS} N_{bulk}}{N_{SERS} I_{bulk}}$$

where I_{SERS} (N_{SERS}) and I_{bulk} (N_{bulk}) are the intensities (the number of BDT molecules probed) for the SERS and bulk spectra, respectively. N_{SERS} was estimated to be 3553 molecules from the foot print of the BDT molecule (0.2 nm^2) and by calculating the total surface area of 20 nm core nanoparticle (1257 nm^2).[5] I_{bulk} and N_{bulk} were determined from the Raman spectra of a 10 mM aqueous BDT solution in 6N NaOH. The following expression was used to approximate the laser spot size (~800 nm in diameter) and the number of BDT molecules in the focal volume:

$$W_0 = \frac{0.61\lambda}{3NA}$$

where W_0 is the minimum waist diameter for a laser beam of wavelength λ focused by an objective with a numerical aperture NA. The focal volume (τ) was approximated from the following expressions.

$$\tau = \left(\frac{\pi}{2}\right)^{1.5} {W_0}^2 Z_0$$

$$Z_0 = \left(\frac{2\pi}{\lambda}\right) {W_0}^2$$

where Z_0 is the focal depth.

1.7 FDTD simulations

FDTD treats Max Well equations as a finite differential equation in the scale of both time and space, and the software package FDTD Solution (version: 8.7.1072, Lumerical Solutions Inc, Vancouver Canada) was used to carry out the FDTD simulations. In the process of computational calculations, the incident light is circularly polarized with the wavelength ranging from 300 to 800 nm and the mesh sizes in x, y, z directions were all fixed to 0.2 nm. Perfectly matched layer (PML) absorbing boundary were used in all directions. To be consistent with the experiments, the surrounding environment (water) of the refractive index was set to be 1.33. All materials used the data from the model of Palik.

In the simulation, the structural model consisted of a 20 nm Au core and an Au shell with thicknesses of 18 nm and 11 nm, separated by a 0.62 nm gap, based on the TEM size statistics before and after etching (Fig. S6). For simplicity, the BRIGHTs were modeled as perfect spheres, and the contribution of 1,4-BDT strands and glass slides was ignored.

2. Supporting Figures

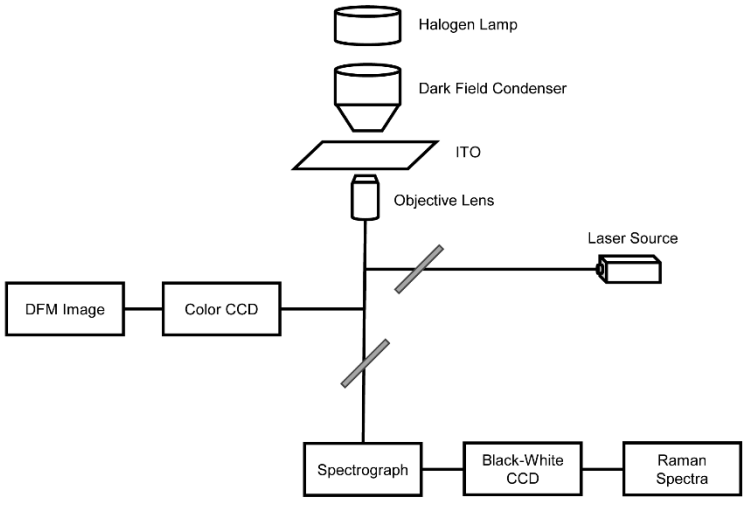

Fig. S1 Schematic diagram of DFM-correlated Raman spectroscopy for in situ single

plasmonic nanostructure detection.

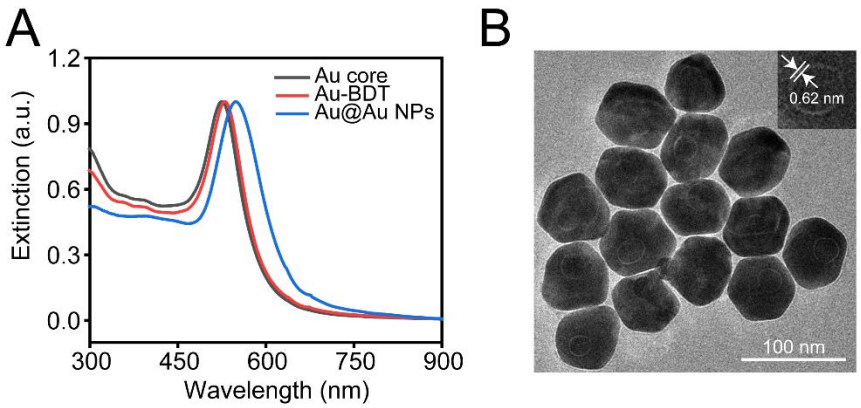

Fig. S2 Characterization of the BRIGHTs. (A) UV-vis extinction spectra of Au core, Au-BDT, and BRIGHTs. (B) Representative TEM image of BRIGHTs. The inset in the upper right corner shows a ~0.62 nm nanoscale gap, corresponding to the length of a single 1,4-BDT molecule.

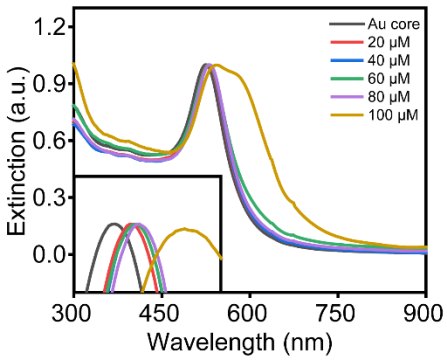

Fig. S3 Optimization of 1,4-BDT concentration. Extinction spectra of Au cores functionalized with the 1,4-BDT at different final concentrations (20, 40, 60, 80, and 100 μM). The spectra show the dependence of the plasmonic peak intensity and position on the molecular loading density. Excessively high 1,4-BDT concentrations led to instability of the Au cores; thus, 80 μM was chosen as the optimal concentration for subsequent experiments.

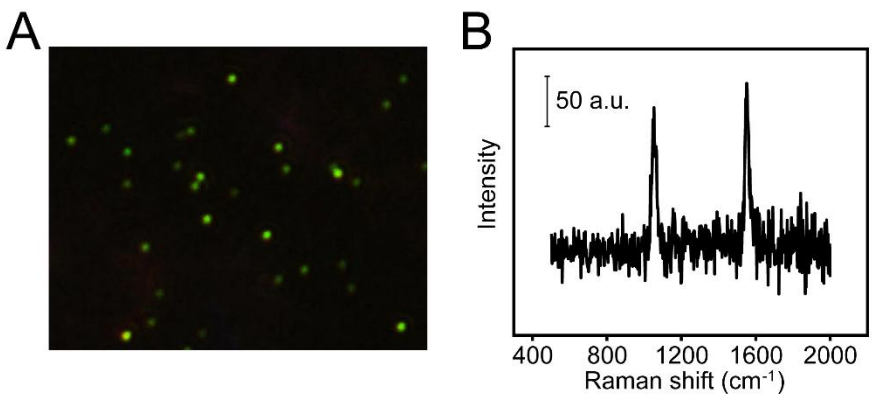

Fig. S4 (A) DFM image of the BRIGHTs on an ITO glass slide. (B) Representative SERS spectra of the individual BRIGHT.

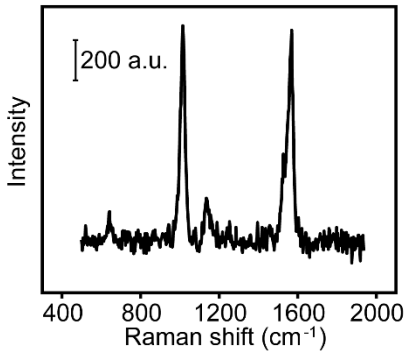

Fig. S5 Normal Raman spectrum of BDT. Normal Raman spectrum of BDT (300 mM) powder showing the characteristic bands at 1555 cm^{-1} employed for estimating the enhancement factor.

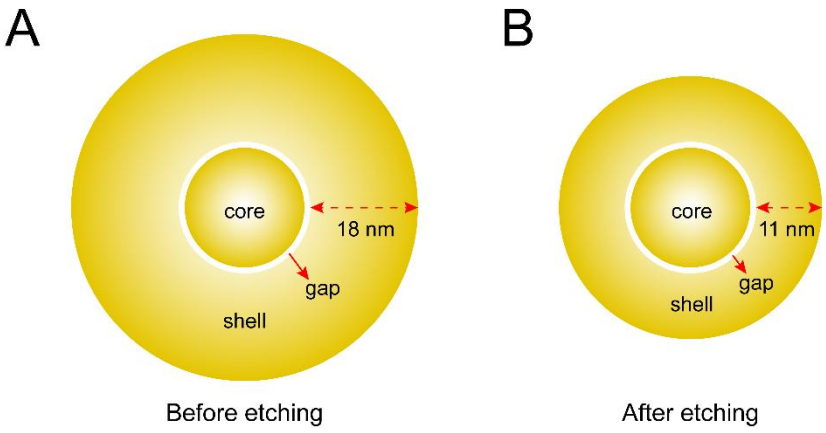

Fig. S6 FDTD simulation models of BRIGHT. The FDTD simulation model of BRIGHT with two different shell thickness.

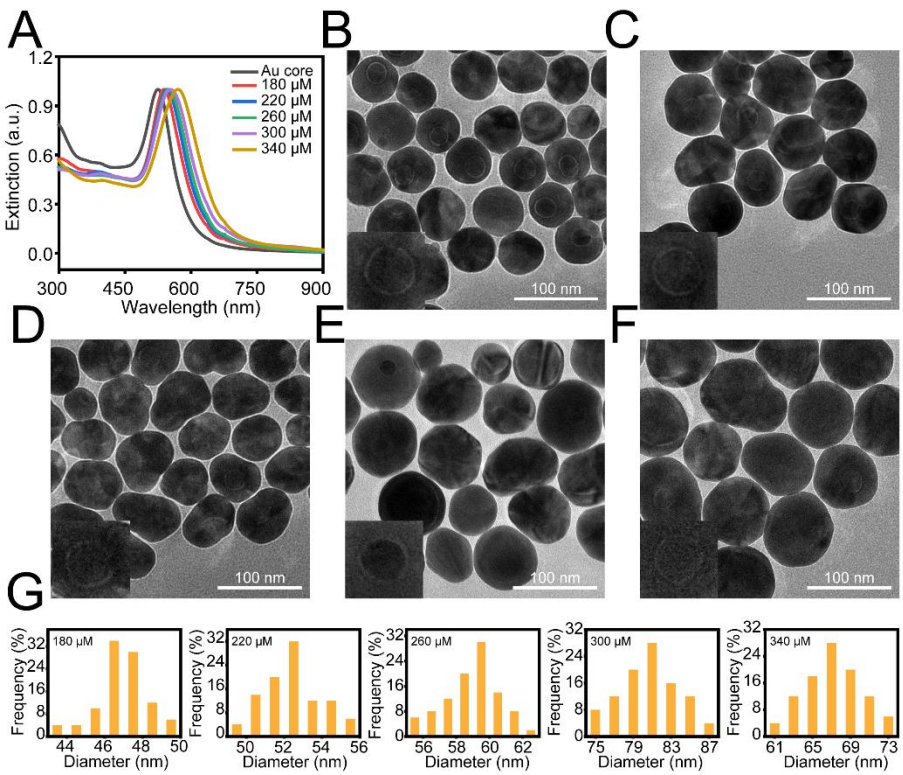

Fig. S7 Extinction spectra of BRIGHTs with different shell thicknesses. (A) Extinction spectra of the core-shell nanoprobes synthesized by adding different final concentrations (180, 220, 260, 300, and 340 μM) of $HAuCl_4$ during the shell growth process. A systematic red-shift of the localized surface plasmon resonance (LSPR) peak is observed with increasing $HAuCl_4$ concentration, indicating a progressive increase in the overall particle size and shell thickness. (B-F) Representative TEM images of the corresponding samples in (A), showing a gradual increase in shell thickness. The inset shows the nanogaps in more detail. (G) Statistical distributions of particle diameters corresponding to samples with different $HAuCl_4$ concentrations.

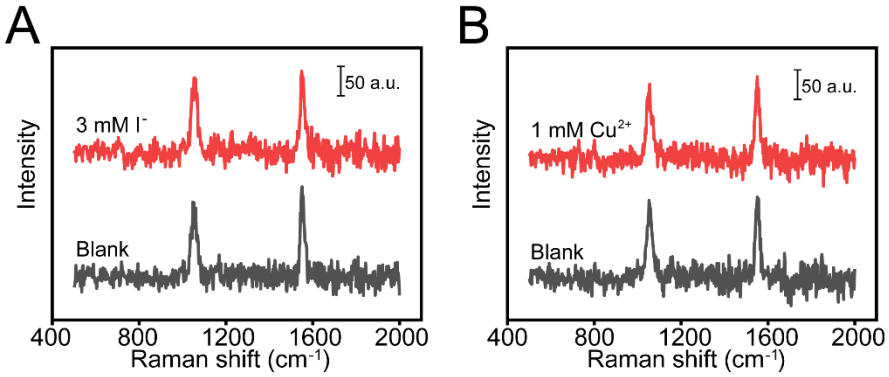

Fig. S8 Effect of iodide and copper ions on the etching reaction. (A) Raman spectra of the probes before (black) and after (red) treatment with 3 mM I^- for 20 min. (B) Raman spectra of the probes before (black) and after (red) treatment with 1 mM Cu^{2+} for 20 min.

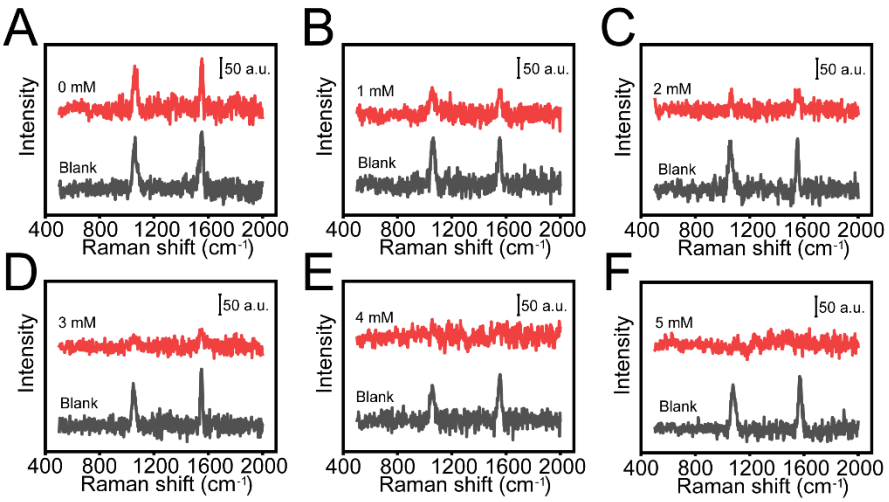

Fig. S9 Optimization of I^- concentration for BRIGHT etching. (A-F) Raman spectra of single BRIGHTs recorded before (black) and after (red) exposure to 1 mM Cu^{2+} in the presence of 0-5 mM I^-. The Raman intensity change depends on the I^- concentration, with 3 mM identified as the optimal condition.

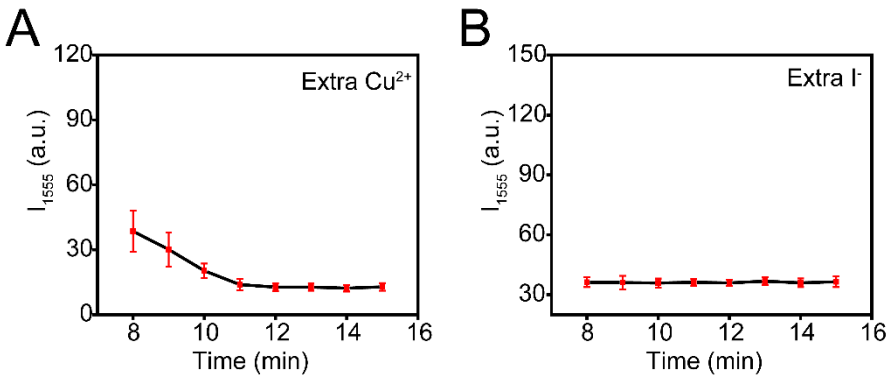

Fig. S10 Time-dependent SERS evolution during the etching reaction. (A) SERS intensity at 1555 cm^{-1} of single BRIGHT upon addition of extra Cu^{2+} at the 8th minute. (B) SERS intensity at 1555 cm^{-1} of single BRIGHT upon addition of extra I^- at the 8th minute.

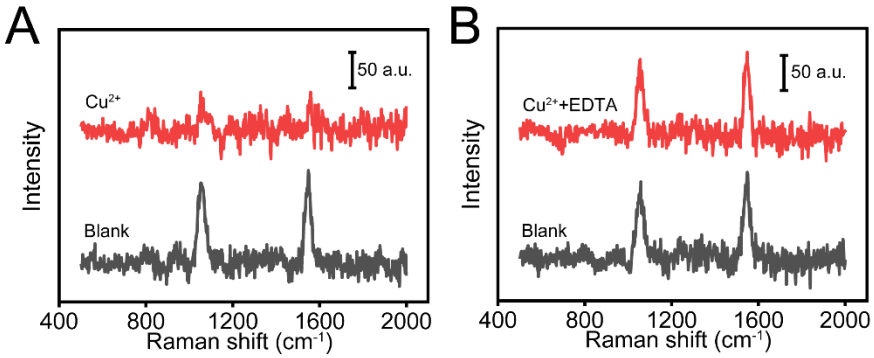

Fig. S11 Proof of concept for Cu^{2+} detection. (A) Raman spectra of a single BRIGHT before (black) and after (red) exposure to 100 μM Cu^{2+}. (B) Raman spectra of a single BRIGHT before (black) and after (red) exposure to a mixture of 100 μM Cu^{2+} and 100 μM EDTA (a metal-ion chelating agent).

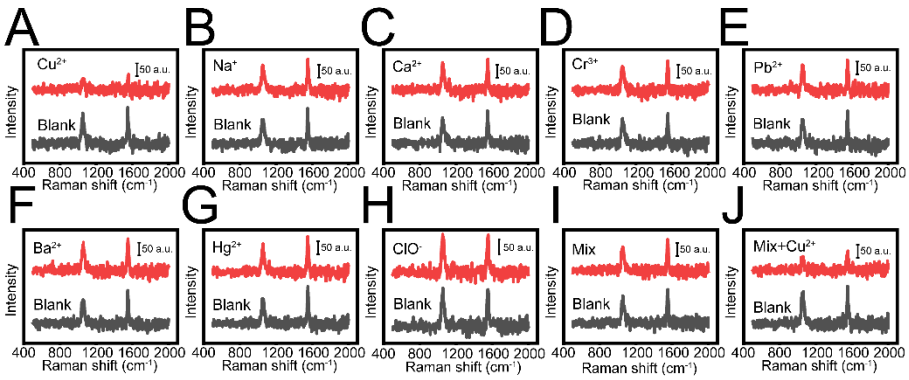

Fig. S12 Selectivity of BRIGHTs probes toward different ions. (A-H) Raman spectra of single BRIGHT recorded before (black) and after (red) exposure to variousions, including Cu^{2+}, Na^{+}, Ca^{2+}, Cr^{3+}, Pb^{2+}, Ba^{2+}, Hg^{2+}, and ClO^{-}. (I) Raman spectra of single BRIGHTs before (black) and after (red) exposure to a mixture of these ions. (J) Raman spectra of single BRIGHTs before (black) and after (red) exposure to the mixed ions in the presence of Cu^{2+}.

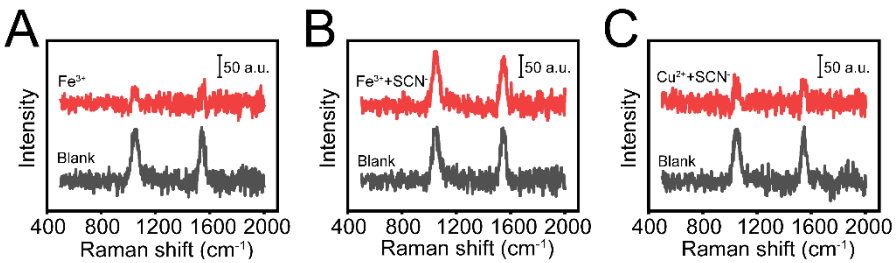

Fig. S13 Verification of Fe^{3+} interference and its suppression by KSCN. (A) Raman spectra of a single BRIGHT nanoprobe before (black) and after (red) exposure to 0.5 mM Fe^{3+}. (B) Raman spectra of a single BRIGHT nanoprobe before (black) and after (red) exposure to Fe^{3+} solution treated with 1 mM KSCN. (C) Raman spectra of a single BRIGHT nanoprobe before (black) and after (red) exposure to Cu^{2+} solution treated with 1 mM KSCN.

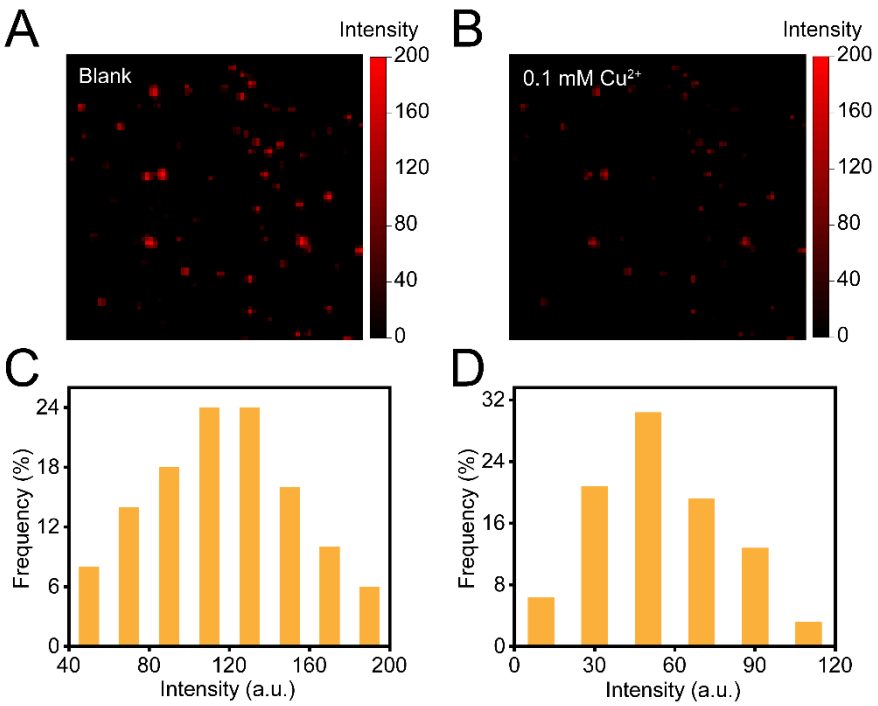

Fig. S14 SERS mapping and statistical analysis of BRIGHT in response to Cu^{2+}. Raman mapping images of BRIGHT in the absence (A) and presence (B) of 0.1 mM Cu^{2+} under the characteristic peak at 1555 cm^{-1}. The corresponding statistical distributions of the SERS intensities are shown in (C) and (D), with the mean intensity decreasing from 122 to 48 counts due to the etching reaction.

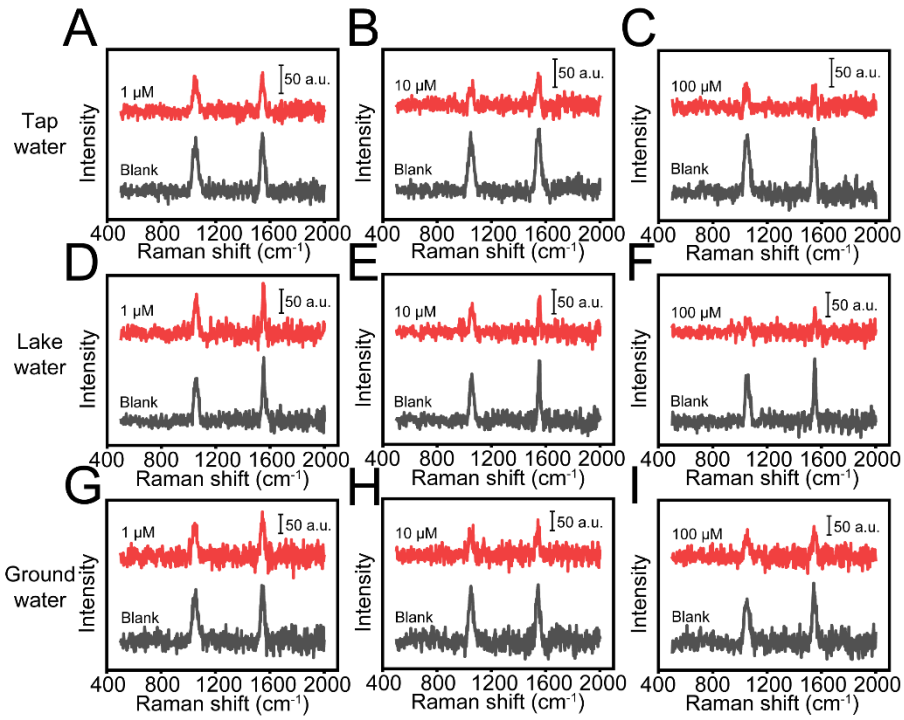

Fig. S15 Detection of Cu^{2+} in complex environmental matrices. Raman spectra demonstrating the response of the nanoprobe to Cu^{2+} at different final concentrations (1, 10, and 100 μM) in various real-world water samples: (A-C) tap water, (D-F) lake water, and (G-I) ground water. The consistent spectral changes across all environments confirm the probe's functionality for Cu^{2+} detection in complex media.

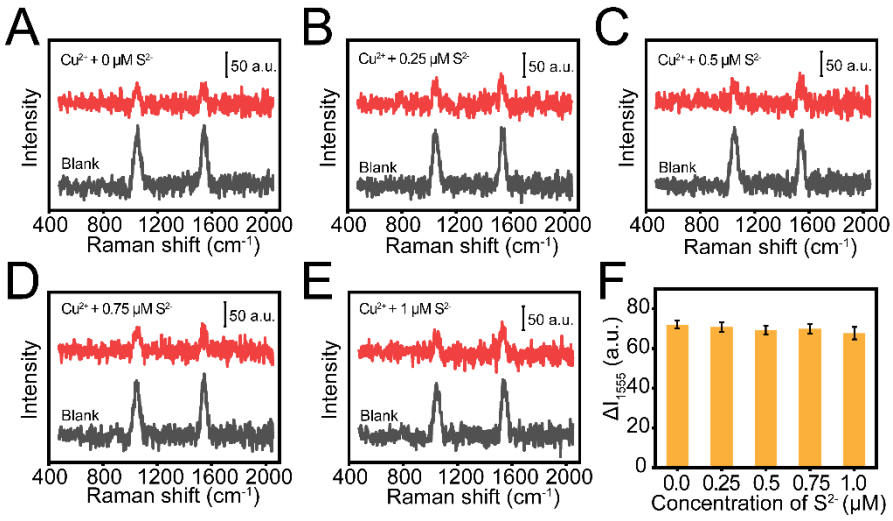

Fig. S16 Evaluation of the influence of sulfide (S^{2-}) on Cu^{2+} detection. (A-E) Raman spectra of a single BRIGHT nanoprobe before (black) and after (red) exposure to

samples containing 0.1 mM Cu^{2+} and 0, 0.25, 0.5, 0.75, and 1.0 μM S^{2-}, respectively. (F) Comparison of the Raman intensity change at 1555 cm^{-1} of BRIGHT in solutions containing different concentrations of S^{2-}.

Table S1 Compare the sensitivity of different techniques to detect Cu^{2+}.

Detection techniques	LOD	Reference
Fluorescent detection	1.6 μM	Ref[6]
Fluorescent protein detection	0.44 μM	Ref[7]
Colorimetric Sensor	2.9 μM	Ref[8]
Fluorescent gold nanoclusters	0.11 μM	Ref[9]
Colorimetric sensor	0.795 μM	Ref[10]
SERS	33.8 nM	This work

References

1 Q. Ruan, L. Shao, Y. Shu, J. Wang and H. Wu, *Adv. Opt. Mater.*, 2013, **2**, 65-73.

2 L. Lin, M. Zapata, M. Xiong, Z. Liu, S. Wang, H. Xu, A. G. Borisov, H. Gu, P. Nordlander, J. Aizpurua and J. Ye, *Nano Lett.*, 2015, **15**, 6419-6428.

3 L. Lin, H. Gu and J. Ye, *Chem. Commun.*, 2015, **51**, 17740-17743.

4 N. Feng, C. Li, J. Shen, Y. Hu, E. K. Fodjo, L. Zhang, S. Chen, Q. Fan and L. Wang, *ACS Nano*, 2022, **16**, 6605-6614.

5 N. Gandra and S. Singamaneni, *Adv. Mater.*, 2012, **25**, 1022-1027.

6 Q. Niu, T. Sun, T. Li, Z. Guo and H. Pang, *Sens. Actuators B Chem.*, 2018, **266**, 730-743.

7 M. Lan, S. Zhao, S. Wu, X. Wei, Y. Fu, J. Wu, P. Wang and W. Zhang, *Nano Res.*, 2019, **12**, 2576-2583.

8 G. J. Park, G. R. You, Y. W. Choi and C. Kim, *Sens. Actuators B Chem.*, 2016, **229**, 257-271.

9 Z. Xu, P. Deng, J. Li and S. Tang, *Sens. Actuators B Chem.*, 2018, **255**, 2095-2104.

10 K. A. Kirk and S. Andreescu, *Anal. Chem.*, 2019, **91**, 13892-13899.